JCTC Journal of Chemical Theory and Computation

Article

pubs.acs.org/JCTC

Reliable Prediction with Tuned Range-Separated Functionals of the Singlet−Triplet Gap in Organic Emitters for Thermally Activated Delayed Fluorescence

Haitao Sun, Cheng Zhong, and Jean-Luc Brédas*

Solar & Photovoltaics Engineering Research Center, Physical Science and Engineering Division, King Abdullah University of Science and Technology (KAUST), Thuwal 23955-6900, Kingdom of Saudi Arabia

Supporting Information

ABSTRACT: The thermally activated delayed fluorescence (TADF) mechanism has recently attracted significant interest in the field of organic light-emitting diodes (OLEDs). TADF relies on the presence of a very small energy gap between the lowest singlet and triplet excited states. Here, we demonstrate that time-dependent density functional theory in the Tamm−Dancoff approximation can be very successful in calculations of the lowest singlet and triplet excitation energies and the corresponding singlet−triplet gap when using nonempirically tuned range-separated functionals. Such functionals provide very good estimates in a series of 17 molecules used in TADF-based OLED devices with mean absolute deviations of 0.15 eV for the vertical singlet excitation energies and 0.09 eV [0.07 eV] for the adiabatic [vertical] singlet−triplet energy gaps as well as low relative errors and high correlation coefficients compared to the corresponding experimental values. They significantly outperform conventional functionals, a feature which is rationalized on the basis of the amount of exact-exchange included and the delocalization error. The present work provides a reliable theoretical tool for the prediction and development of novel TADF-based materials with low singlet−triplet energetic splittings.

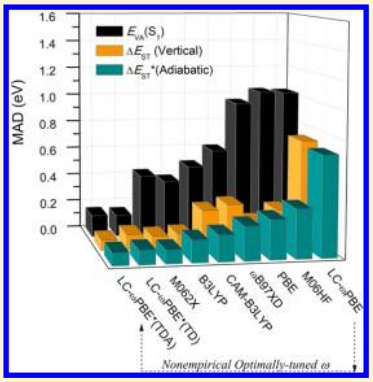

1. INTRODUCTION

Organic π-conjugated molecules substituted by appropriate donor and acceptor groups (D/A) are known to exhibit interesting optoelectronic properties[1] due to their significant charge-transfer (CT) characteristics upon photoexcitation. Such compounds have attracted considerable attention in particular in the fields of organic nonlinear optics,[2] organic field-effect transistors,[3] and organic photovoltaic cells.[4,5] Recently, donor−acceptor structural arrangements have also been key in the development of thermally activated delayed fluorescence (TADF)[6−10] materials, which represent the third generation of organic light-emitting diodes (OLEDs).[11]

In OLEDs, electrons injected from a cathode and holes injected from an anode recombine into luminescent molecules in the active layer and bring them in their excited states. When spin statistics are obeyed, this process leads to formation of a triplet excited state 75% of the time and to a singlet excited state 25% of the time. In the case of purely organic molecules, the triplet excited state is dark, and the maximum internal quantum efficiency is then limited to 25%. However, when the energy gap (ΔE_{ST}) between the lowest singlet (S_1) and triplet (T_1) excited states is small enough, up-conversion from T_1 to S_1 can take place with the assistance of thermal energy. Ideally, all of the triplet excitons (75%) should be able to convert to S_1 and fluoresce, which can lead to an internal quantum efficiency close to 100% (Figure 1).[12] Adachi and co-workers have demonstrated that a very small ΔE_{ST} is essential, although not sufficient, to achieve efficient TADF via such a $T_1 \rightarrow S_1$ reverse intersystem crossing (ISC).[6,13] A small ΔE_{ST} can usually result from spatial separation between the highest occupied molecular orbital (HOMO) and the lowest unoccupied molecular orbital (LUMO).[14]

Despite their potential usefulness in this emerging field, theoretical investigations of the excited states and excitation spectra of TADF-based materials remain relatively limited and have proven to be challenging. A main issue from a theoretical perspective is finding the appropriate level of theory capable of providing both efficient (qualitative) and accurate (quantitative) predictions of the electronic structures of large charge-transfer-type molecules.[15] Indeed, TADF molecules often consist of >100 atoms, which limits their studies with high-level methods, such as post-Hartree−Fock (PHF) techniques[16] or many-body perturbation theory at the GW-BSE level.[17] Available experimental data for TADF molecules indicate that the singlet−triplet splitting ΔE_{ST} can be as small as 0.1 eV,[10] which requires that the theoretical methodologies be able to provide quantitative predictions.

Conversely, time-dependent density functional theory (TDDFT)[18,19] is a well-established tool to study the excited states of relatively large molecular systems and affords a reasonable compromise between accuracy and computational cost.[20] However, when dealing with donor−acceptor molecules with CT characteristics, TDDFT calculations based on standard

Received: May 11, 2015
Published: July 9, 2015

DOI: 10.1021/acs.jctc.5b00431
J. Chem. Theory Comput. 2015, 11, 3851−3858

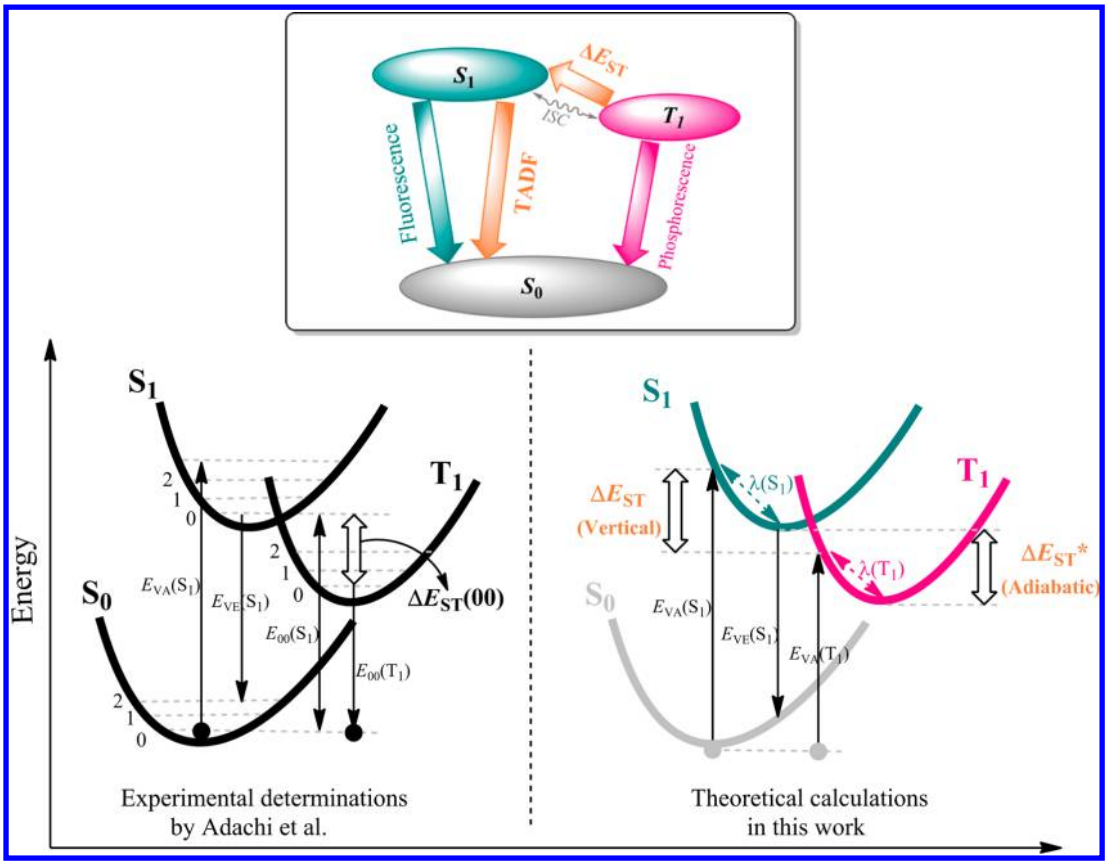

Figure 1. Schematic representation (top) and potential energy surfaces (bottom) of the photophysical processes in thermally activated delayed fluorescence (TADF) compounds. S_0: singlet ground state; S_1: lowest singlet excited state; T_1: lowest triplet excited state; ISC: intersystem crossing. VA: vertical absorption; VE: vertical emission; $\lambda(S_1)$ and $\lambda(T_1)$: relaxation energies of S_1 and T_1, respectively.

functionals can severely underestimate the excitation energies.[21] In general, these systematic errors can be attributed to the introduction of inappropriate exchange-correlation (XC) approximations and can be further traced back to large electron self-interaction or delocalization error (DE)[22,23] and a lack of derivative discontinuity (DD),[24] as well as to an incorrect behavior of the electron−electron potential at asymptotically large distances.[25,26] The introduction of a suitable, fixed amount of exact-exchange (eX) has been shown to provide an improved description of the excited-state properties.[10] The vertical transition energies of the first singlet states in TADF molecules and the (closely related) electronic-coupling (or transfer-integral) parameters in organic molecular crystals have been shown to be very sensitive to the amount of eX.[10,27,28] Thus, an appropriate balance between the eX from Hartree−Fock and electron correlation from DFT is crucial to achieve reliable estimates of π-conjugated electronic structures.[29] As such, the issue becomes how to determine such a balance and how much eX should be included for a specific system.

Recently, the development of range-separated exchange (RS)[30] density functionals has allowed the mitigation of the CT issue with TDDFT.[29,31,32] The general expression of RS functionals provides a theoretical framework based on which one can adjust the parameters in eq 1 to tune the percentages of eX. In such functionals, a three-parameter expression of the interelectronic distance r_{12} is used for the separation of the exchange term into a short-range domain and a long-range domain[25]

$$\frac{1}{r_{12}} = \frac{1 - [\alpha + \beta \mathrm{erf}(\omega r_{12})]}{r_{12}} + \frac{\alpha + \beta \mathrm{erf}(\omega r_{12})}{r_{12}} \quad (1)$$

Thus, the exchange term is split into a long-range eX component coming from Hartree−Fock and a short-range DFT component derived from local-density or generalized-gradient approximations (LDA or GGA). The parameter α quantifies the fraction of eX in the short-range limit, whereas $\alpha + \beta$ gives the fraction of eX in the long-range limit. The range-separation parameter ω represents the inverse of the distance at which the exchange term switches from DFT- to HF-like. The ω values in RS functionals have been shown to be strongly system-dependent, in particular in the case of π-conjugated systems.[33−35] Baer, Kronik, and their collaborators have considered a nonempirical criterion to determine the optimal ω in RS functionals.[36] The concept of "optimal tuning" corresponds to adjusting ω to fulfill a fundamental property that the exact functional must obey in exact Kohn−Sham (KS) or generalized KS (GKS) theory: for an N-electron system, the negative of the HOMO energy $-\varepsilon_H(N)$ must equal the molecular vertical ionization potential (IP).[37] For a given system, the optimal ω value can hence be obtained without empirical fitting by minimizing expression 2a.

$$J = |\varepsilon_H(N) + IP(N)| \quad (2a)$$

In donor−acceptor systems, it is useful to focus not only on the ionization potential (essentially related to the donor component) but also on the electron affinity (essentially related to the acceptor component). The vertical electron

DOI: 10.1021/acs.jctc.5b00431
J. Chem. Theory Comput. 2015, 11, 3851−3858

Scheme 1. Chemical Structures of the Molecules Investigated in This Work with the Experimental Singlet-Triplet Gaps Taken from the Work of Adachi and Co-Workers[10]

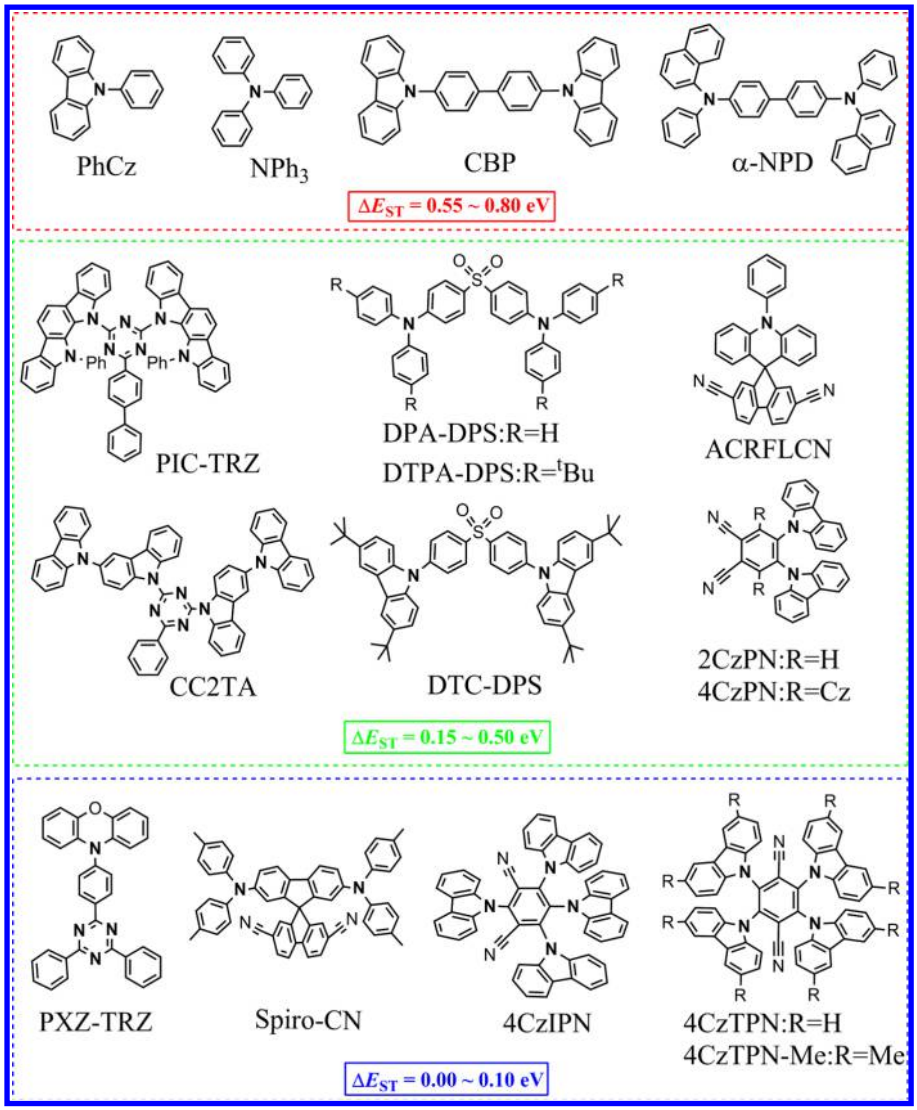

affinity (i.e., in the absence of geometry relaxation) of the N-electron system can be considered as the ionization potential of the $N + 1$ electron system. In this context, the tuning of the ω value can be done on the basis of expression 2b.[38]

$$J^2 = \sum_{i=0}^{1} [\varepsilon_H(N + i) + IP(N + i)]^2 \quad (2b)$$

which is used throughout this work. The optimally tuned range-separated DFT method has been successfully used in cases generally considered challenging for TDDFT.[22,23] In addition, the Tamm−Dancoff approximation (TDA)[39−41] scheme of TDDFT has been recently shown to provide reliable absorption and emission spectra[42] and especially better estimates of the lowest singlet−triplet energy gaps,[43] which is relevant for TADF systems.

In this work, our goal is to demonstrate the predictive ability of TD(A)DFT calculations using nonempirically tuned RS functionals for the vertical (absorption) excitation energies of the first singlet excited states $E_{VA}(S_1)$ and the corresponding singlet−triplet gaps ΔE_{ST}. The calculations are carried out for a series of 17 molecules whose chemical structures are shown in Scheme 1. This series consists of (i) 4 molecules with relatively large singlet−triplet gaps (ΔE_{ST} = 0.55−0.80 eV), usually used as hole/electron transporting layers; (ii) 8 molecules with moderate gaps (ΔE_{ST} = 0.15−0.50 eV); and (iii) 5 molecules with very small gaps (ΔE_{ST} = 0.00−0.10 eV), which can be considered representative TADF emitters. All these molecules are typical donor−acceptor CT molecules, mainly based on fragments such as carbazolyl (Cz), triphenylamine (NPh_3), 1,3,5-triazine (TRZ), or dicyanobenzene (DCB). The molecular structures are such that adjacent donor and acceptor units, due to steric hindrance, can be strongly out of plane. Therefore, such structures are prone to lead to spatial separations of HOMOs and LUMOs, which can lead to small ΔE_{ST} values. We note that calculations using conventional functionals are also performed for the sake of comparison.

2. COMPUTATIONAL DETAILS

Ground-state geometries for all of the molecules collected in Scheme 1 (taken from the work by Adachi et al.[10]) are optimized at the B3LYP/6-31G(d) level. The optimal ω values were determined based on the LC-ωPBE functional with the 6-31+G(d) basis set and are listed in Table 1. Hereafter, we refer

DOI: 10.1021/acs.jctc.5b00431
J. Chem. Theory Comput. 2015, 11, 3851−3858

Table 1. Calculated $E_{VA}(S_1)$ and $E_{VA}(T_1)$ Values and Vertical Singlet-Triplet Gaps ΔE_{ST} and Adiabatic Singlet-Triplet Gaps ΔE_{ST}* in Comparison to Experimental Data

			PCM(toluene)-TDA-DFT/6-31+G(d) level							
			LC-ωPBE (ω = 0.400)			LC-ωPBE*			exp. values[b]	
	compound	ω*[a]	$E_{VA}(S_1)$	ΔE_{ST}	ΔE_{ST}*	$E_{VA}(S_1)$	ΔE_{ST}	ΔE_{ST}*	$E_{VA}(S_1)$	$\Delta E_{ST}(00)$
L	PhCz	0.204	4.66	1.20	1.19	4.17	0.73	0.75	3.66	0.55
	NPh_3	0.198	4.71	1.21	1.22	3.98	0.61	0.74	3.74	0.57
	CBP	0.173	4.62	1.26	1.33	3.94	0.66	0.88	3.80	0.71
	α-NPD	0.170	4.17	1.31	1.51	3.29	0.57	0.76	3.31	0.73
M	PIC-TRZ	0.141	4.28	1.09	0.91	3.17	0.22	0.11	3.35	0.18
	DPA-DPS	0.166	4.33	1.04	0.98	3.60	0.60	0.49	3.53	0.52
	DTPA-DPS	0.152	4.28	1.02	1.11	3.48	0.56	0.46	3.47	0.46
	ACRFLCN	0.174	4.52	1.50	1.35	3.03	0.07	0.02	3.05	0.24
	CC2TA	0.159	4.54	1.14	0.86	3.66	0.35	0.13	3.64	0.20
	DTC-DPS	0.160	4.51	1.09	1.27	3.60	0.39	0.27	3.62	0.36
	2CzPN	0.176	4.20	1.06	1.24	3.22	0.41	0.24	3.19	0.31
	4CzPN	0.146	3.96	0.92	1.02	2.55	0.13	0.00	2.82	0.15
S	PXZ-TRZ	0.183	4.10	0.94	0.60	2.94	0.07	0.01	2.73	0.06
	Spiro-CN	0.168	3.97	1.08	0.89	2.73	0.07	0.01	2.69	0.06
	4CzIPN	0.142	3.84	0.75	0.73	2.52	0.12	0.01	2.85	0.10
	4CzTPN	0.147	3.63	0.59	0.70	2.32	0.14	0.06	2.61	0.09
	4CzTPN-Me	0.143	3.69	0.63	0.43	2.28	0.12	0.09	2.49	0.09
	MAD[c]		1.03	0.73	0.70	0.15	0.07	0.09		

[a]Optimal range-separation parameter ω* (Bohr^{-1}) used in the LC-ωPBE* calculations. [b]Experimental data are taken from ref 10. [c]The MAD values are calculated with respect to the corresponding experimental values. The labels L, M, and S refer to molecules with relatively large, medium, and small singlet−triplet gaps, respectively.

to the optimally tuned functional as LC-ωPBE*. The optimal ω values appear not to be sensitive to extension of the basis set from 6-31G(d) to 6-31+G(d) (Table S1 in Supporting Information (SI)). For the optimization of the range-separation parameter ω, all the single-point calculations were carried out for the N and $N \pm 1$ systems using the default SCF convergence criteria in the Gaussian 09 code.[44] An original "Golden proportion" approach (see SI for details) was developed to obtain the optimal ω value that minimizes J^2 in eq 2b (note that the search for optimal ω values was limited to the range 0.05−0.5 Bohr^{-1}).

The vertical excitation (absorption) energies of the lowest singlet- ($E_{VA}(S_1)$) and triplet- ($E_{VA}(T_1)$) excited states are calculated using linear-response TDDFT or the TDA approach with the 6-31+G(d) basis set. The vertical singlet−triplet splitting is accordingly obtained as $\Delta E_{ST} = E_{VA}(S_1) - E_{VA}(T_1)$. To take into account the effects of the dielectric medium, we have tested the polarizable continuum model (PCM)[45] using the default linear-response method as well as the recently developed state-specific (SS) approach[46] in the calculations of excitation energies, as shown in Table S2 in the SI. We find that, while requiring additional computational effort, the SS method does not produce any significant improvement in the prediction of the $E_{VA}(S_1)$ values compared to the linear-response method. Therefore, the PCM approach using the default linear-response method is employed in the calculations of excitation energies discussed in this work.

The basis-size effects were examined by extending the basis sets from 6-31G(d) to 6-31+G(d), 6-311G(d), 6-311+G(d), and 6-311++G(d,p) (see Table S2 (SI)). The 6-31+G(d) basis shows a good balance between accuracy of the results and reasonable computational cost. It should be noted that most of the experimental ΔE_{ST} values are deduced from delayed fluorescence or phosphorescence spectra taken in solution (usually in toluene); therefore, they are related to $E_{00}(S_1)$ and $E_{00}(T_1)$, which involve excited-state geometry relaxations, as shown in Figure 1. We thus carried out calculations of the adiabatic ΔE_{ST}* values, which are defined as the energy differences between the minima potential energies of the S_1 and T_1 states. The geometries of the S_1 states are optimized using the implemented TDDFT gradients at the PCM (toluene)-CAM-B3LYP/6-31G(d) level; the geometries of the T_1 states are assessed by spin-relaxed open-shell optimizations at the UCAM-B3LYP/6-31G(d) level (also considering toluene as the dielectric medium). The reason we employed the CAM-B3LYP functional is related to the fact that the TADF molecules considered here are mostly donor−acceptor charge-transfer molecules and B3LYP would significantly overestimate electron delocalization in the excited states. The results in Table S3 (SI) show that, in comparison to full TDDFT, the corresponding TDA approach with tuned LC-ωPBE* functionals gives a slightly improved description of the singlet−triplet splittings (ΔE_{ST}) with respect to the experimental data due to the better description of the triplet excitation energies within the TDA approach.[43] Considering its lower computational cost and the possibility of avoiding the triplet instability issue,[42] the TDA scheme is employed here for all of the calculations of excitation energies. Therefore, except when explicitly stated otherwise, all ΔE_{ST} calculations were carried out at the PCM (toluene)-TDA-DFT/6-31+G(d) level.

To examine to what extent the TDA results based on ground-state geometries optimized with different functionals change, we have calculated the singlet and triplet excitation energies using the optimally tuned LC-ωPBE* functional based on the ground-state geometries optimized with LC-ωPBE*, B3LYP, and CAM-B3LYP, and compared the results to the corresponding experimental data (see Table S4 (SI)). We find that the calculated excitation energies remain close regardless of the functionals used for the ground-state geometry optimizations. This finding is consistent with recent studies by Tamblyn

DOI: 10.1021/acs.jctc.5b00431
J. Chem. Theory Comput. 2015, 11, 3851−3858

et al.[47] and Adachi et al.[10] To test the performance of various density functionals and the influence of eX percentages (eX%), we performed calculations with seven functionals at different levels of Perdew's Jacob's ladder:[48] a pure GGA functional, PBE[49] (0%); a hybrid-GGA functional, B3LYP[50,51] (20%); two meta-GGA functionals, M062X[52] (56%) and M06HF[53] (100%); and three range-separated functionals, CAM-B3LYP[25] (α = 0.19, $\alpha+\beta$ = 0.65, short-range ∼ long-range: 19∼65%), LC-ωPBE[54] (α = 0.0, $\alpha+\beta$ = 1.0, 0∼100%), and ωB97XD[31,55] (α = 0.22, $\alpha+\beta$ = 1.0, 22∼100%). Figure 2 displays the percentage of eX included as a function of interelectronic distance (r_{12}) for various functionals. Recent results[43] using double-hybrid density functionals that lie on the top level of the DFT "ladder" are also included in the discussion for the sake of comparison.

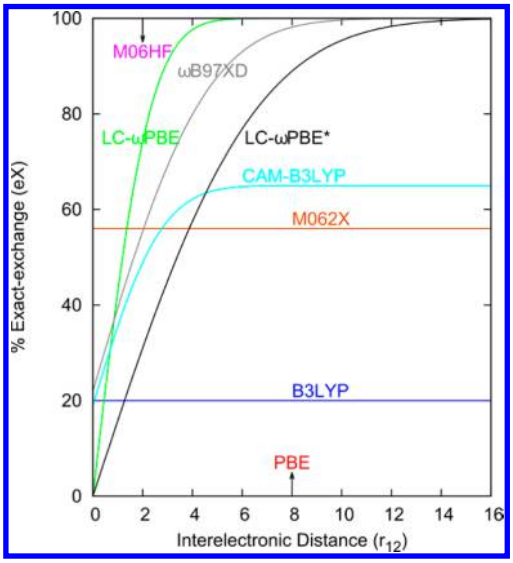

Figure 2. Percentage of exact-exchange (eX) included as a function of interelectronic distance (r_{12}, Bohr) for various functionals. The LC-ωPBE* curve is taken from the calculation on PIC-TRZ with an optimal ω value of 0.141 Bohr^{-1}.

3. RESULTS AND DISCUSSION

Table 1 lists the optimal ω values, the calculated vertical absorption energies $E_{VA}(S_1)$, the vertical ΔE_{ST}, and adiabatic ΔE_{ST}* values and their mean absolute deviation (MAD) values using the LC-ωPBE* and nontuned LC-ωPBE results relative to the experimental data. For comparison, detailed results using the other density functionals are reported in Table S6 (SI). The optimal ω values are in the range from 0.141 (PIC-TRZ) to 0.204 (PhCz) Bohr^{-1}; they are thus significantly smaller than the default ω value for LC-ωPBE (0.400 Bohr^{-1}), indicating that the tuned functional switches from DFT to eX at larger interelectronic distances. In other words, the short-range DFT component is more slowly replaced by eX. These results confirm the necessity of "tuning" ω because smaller ω values are required for a proper description of the TADF molecules in this work. The default parameters for other popular RS functionals (0.330 Bohr^{-1} for CAM-B3LYP and 0.200 Bohr^{-1} for ωB97XD) are still (somewhat) larger than is optimal. Our results in Table 1 show that, in comparison to the nontuned LC-ωPBE functional (with MADs of 1.03 eV for $E_{VA}(S_1)$, 0.73 eV for ΔE_{ST}, and 0.70 eV for ΔE_{ST}*), the corresponding optimally tuned version can significantly reduce the errors by up to 1 order of magnitude, with MADs of 0.15 eV for $E_{VA}(S_1)$, 0.07 eV for ΔE_{ST}, and 0.09 eV for ΔE_{ST}*.

In Table 2, the results of statistical analyses including the MADs, relative errors (RE), and linear correlation coefficients (R^2) between the theoretical and experimental data are collected for the other functionals considered in this work. The histograms in Figures S1−S3 (SI) are also plotted for better visualization of the error distributions. For the lowest singlet excitation energies, except for the pure GGA PBE and hybrid B3LYP, all of these functionals consistently overestimate the $E_{VA}(S_1)$ values. PBE with 0% eX and the meta-GGA M06HF with 100% eX produce very large MADs of 0.95 and 1.04 eV, respectively, and relatively large percentages of RE of 31 and 34%, respectively. The hybrid B3LYP and M062X functionals, which include a fixed amount of eX, reduce the MADs and REs by about half (0.39 and 0.43 eV; 13 and 14%; respectively), which confirms the pivotal effect of considering an "optimal" percentage of exact exchange in the electronic-structure methodology.[10,43] The untuned RS functionals, such as CAM-B3LYP and ωB97XD, produce slightly greater errors compared to the hybrid B3LYP and M062X functionals. Except for PBE and M06HF, all the functionals provide a reasonably high linear correlation coefficient R^2 (0.80−0.97) between the calculated and experimental data.

For the singlet−triplet gaps, we first analyze the performance of functionals in the prediction of the vertical ΔE_{ST} values and then turn to the adiabatic ΔE_{ST}* values, which include relaxation effects. It should be noted that, in comparison to the pure GGA and hybrid GGA functionals, all the RS functionals produce rather large MADs (0.26−0.73 eV) and REs (144∼473%). The B3LYP and M062X functionals seem to

Table 2. Statistical Analysis Including Mean Absolute Deviations (MAD, eV), Relative Errors (RE), and Linear Correlation Coefficients (R^2) Obtained from the Comparison between Theoretical and Experimental Data[a]

	$E_{VA}(S_1)$			ΔE_{ST}			ΔE_{ST}*		
functional	MAD	RE (%)	R^2	MAD	RE (%)	R^2	MAD	RE (%)	R^2
PBE	0.95	31	0.67	0.17	52	0.50	0.28	105	0.22
B3LYP	0.39	13	0.87	0.10	36	0.73	0.16	73	0.74
M062X	0.43	14	0.96	0.09	48	0.85	0.10	57	0.89
M06HF	1.04	34	0.72	0.25	197	0.27	0.34	228	0.38
CAM-B3LYP	0.49	16	0.97	0.26	144	0.77	0.19	71	0.94
ωB97XD	0.61	19	0.94	0.30	187	0.69	0.24	101	0.91
LC-ωPBE	1.03	33	0.80	0.73	473	0.31	0.70	409	0.57
LC-ωPBE*	0.15	5	0.91	0.07	27	0.85	0.09	41	0.93

[a]MAD = $(1/n)\sum_i^n|\Delta E_{cal} - \Delta E_{exp}|$ and RE = $(1/n)\sum_i^n|((\Delta E_{cal} - \Delta E_{exp})/\Delta E_{exp})|$.

DOI: 10.1021/acs.jctc.5b00431
J. Chem. Theory Comput. 2015, 11, 3851−3858

produce small deviations (0.09−0.10 eV). The good performance using M062X functional is also observed by Jacquemin and collaborators.[56] However, when considering the relatively large MADs of the $E_{VA}(S_1)$ values using B3LYP (0.39 eV) and M062X (0.43 eV), their small MADs are mainly attributed to an error cancellation resulting from the simultaneous under-/overestimation of singlet and triplet excitation energies. For the description of the ΔE_{ST}* values, all the functionals show similar performance as for the vertical ΔE_{ST} values. It is worth noting that negative ΔE_{ST}* values are observed using PBE and B3LYP (as shown in Table S6 (SI)), which results in significantly larger MADs and REs in comparison to the results for the vertical ΔE_{ST}. Overall, the functionals adopting conventional XC approximations give inconsistent results in going from one system to another, which calls into question their reliability in the prediction of the properties of new TADF molecules. Importantly, the optimally tuned LC-ωPBE* functional delivers both the smallest MADs (0.15 eV for $E_{VA}(S_1)$, 0.07 eV for vertical ΔE_{ST}, and 0.09 eV for adiabatic ΔE_{ST}*) and lowest REs (5%, 27%, and 41%) and also comes with high R^2 values (0.91, 0.85, and 0.93). In addition, the plots of error distributions present a Gaussian shape with a peak position around zero (see Figures S1−S3 (SI)), which demonstrates the reliability of an optimally tuned RS functional.

A recent study by Moral et al.[43] using "state-of-the-art" double-hybrid functionals (B2-PLYP and B2GP-PLYP) shows that the MADs for the $E_{VA}(S_1)$ values collected for six selected molecules (PhCz, NPh_3, ACRFLCN, CBP, 2CzPN, and PXZ-TRZ) are 0.34 and 0.28 eV, respectively. Thus, it appears that the errors are not significantly reduced compared to those of the tuned functional. The errors between the calculated $E_{VA}(S_1)$ values using LC-ωPBE* and experimental values and their distributions are presented in Table 1 and Figure S1 (SI). It can be seen that for 8 of the 17 molecules studied in this work, the differences are <0.1 eV, and for 8 other ones, they are in the range of roughly 0.1−0.3 eV. All these errors distribute as a Gaussian with the peak around zero. Interestingly, there is one molecule, PhCz, for which a larger error of 0.51 eV is found with a calculated $E_{VA}(S_1)$ value of 4.17 eV compared to an experimental estimate of 3.66 eV. Thus, we also performed high-level calculations of the vertical singlet excitation energy in PhCz with second-order approximate coupled-cluster (CC2) theory and considered the results using double-hybrid functionals taken from the work of Moral et al.[43] As shown in Table S5 (SI), the results from the high-level methods are close to those from tuned LC-ωPBE* (CC2: 3.98 eV, B2-PLYP: 3.98 eV, and B2GP-PLYP: 4.15 eV). It is clearly of interest to employ such well-established, reliable, high-level methods to benchmark the excitation energies for TADF molecules; however, their main challenge comes from their very high computational costs when the molecular size becomes large. That a comparable level of accuracy is obtained when using the optimal-tuning approach again confirms its clear benefit given its relatively low computational cost. By taking into account the overall performance of the representative functionals selected from the Jacob's ladder of DFT, the optimally tuned RS functional significantly outperforms all the other types of functionals and achieves excellent accuracy at reasonable computational cost.

To analyze the extent of excited-state geometry relaxations, we present the relaxation energies $\lambda(S_1)$ and $\lambda(T_1)$ for the S_1 and T_1 states, respectively, in Figure 1 and Table S7 (SI). The relaxation effects are seen to be system-dependent with the mean values for $\lambda(S_1)$ and $\lambda(T_1)$ collected for all 17 molecules being 0.17 and 0.13 eV, respectively. It is worthwhile to recall that extended, linear, π-conjugated molecules have similar relaxation energies in the S_1 state but usually display substantially larger relaxations in the T_1 state (due to a stronger localization of the T_1 wave function), which leads to ΔE_{ST} values in the range of 0.7−1.0 eV.[57,58] Interestingly, the molecules with a large ΔE_{ST} are those where small $\lambda(S_1)$ values are accompanied by larger $\lambda(T_1)$ values. Conversely, the molecules with small ΔE_{ST} possess relatively larger $\lambda(S_1)$ values, indicating more pronounced geometry relaxation in the S_1 state. We then plot the hole/electron distributions of S_1 and T_1 for the two representative molecules: CBP ($\lambda(S_1)$ = 0.18 eV and $\lambda(T_1)$ = 0.40 eV) and CC2TA ($\lambda(S_1)$ = 0.29 eV and $\lambda(T_1)$ = 0.07 eV) in Scheme S1 of the SI. A more localized character is found in the T_1 state of CBP and the S_1 state of CC2TA. As shown in Table S8 (SI), all S_1 transitions are characteristic of typical CT excitations. For the T_1 states, our results show a significant local-excitation (LE) character; this is in agreement with the experimental assignments, except for PIC-TRZ, 4CzPN, and 4CzIPN[10] (it should be borne in mind, however, that it may be difficult to make accurate assignments of the T_1 states when the experimental bands show a poorly defined shape with low resolution).

Next, from the perspective of the eX percentages included in the investigated functionals, we try to analyze the reason why different functionals produce different sizes of error. As seen in Figure 2, at r_{12} values between 2.5 and 3 Bohr (roughly 1.322−1.587 Å), which is the range of carbon−carbon single and double bonds, the LC-ωPBE* functional affords roughly 45% eX whereas the nontuned LC-ωPBE with a default ω of 0.4 gives almost 90% eX, which points to LC-ωPBE as being HF-like; at similar distances, the CAM-B3LYP and ωB97XD functionals contain roughly 60 and 70% eX, respectively. These percentages of eX included in the functionals are found to be consistent with the size of the errors; in other words, the higher the eX %, the greater the errors, which confirms the findings of Mortal et al.[43] It can be concluded that the overall overestimation of $E_{VA}(S_1)$ and ΔE_{ST} with commonly used RS functionals is related to their more HF-like character. In this regard, the slightly better performance of B3LYP and M062X can also be attributed to a suitable amount of eX.

It has been shown that the problems posed by TDDFT are closely related to violations of basic conditions of constraints.[59] In exact Kohn−Sham theory, the energy of an atom or molecule as a function of electron number $E(N)$ should afford straight-line segments between integers. However, commonly used functionals with inappropriate XC kernels tend to over/underestimate the delocalization effect of holes/electrons and produce a so-called DE. This error can be quantitatively characterized by the curvature of $E(N)$ as shown in Figure 3. Here, the behavior of $E(N)$ is examined for PhCz as a representative example. The results are as expected: the pure GGA PBE and global hybrid B3LYP functionals produce large positive curvatures of $E(N)$, indicating that these functionals provide too delocalized wave functions. Magnitude-wise, the M062X and CAM-B3LYP functionals produce a less pronounced DE compared to conventional PBE and B3LYP. Interestingly, for the M06HF and LC-ωPBE functionals, the DEs are also improved but afford obvious negative curvatures, indicating a somewhat too localized, HF-like character. Overall, the optimally tuned LC-ωPBE* reduces the DE to a minimum. The results confirm that reducing the delocalization error and

DOI: 10.1021/acs.jctc.5b00431
J. Chem. Theory Comput. 2015, 11, 3851−3858

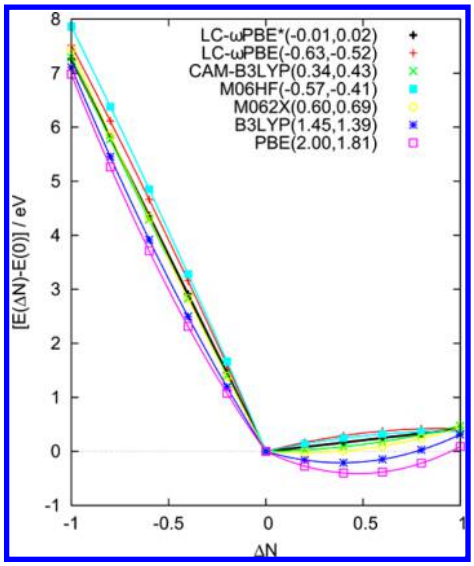

Figure 3. Energy of the PhCz molecule as a function of the fractional electron number (ΔN) relative to the neutral system ($\Delta N = 0$). The numerical values in the plot correspond to the coefficients of $(\Delta N)^2$ of quadratic fits to $E(N)$ in the electron-deficient and -rich regime, respectively ($\Delta N < 0$, $\Delta N > 0$). The calculations are performed using the developmental version of the NWChem package.[61]

thus the many-electron self-interaction error is an additional indicator to select the optimal functionals.[22,60]

4. CONCLUSIONS AND OUTLOOK

We have demonstrated the efficiency of a nonempirically tuned range-separated exchange functional in reproducing the experimental lowest singlet excitation energies and the corresponding singlet−triplet gaps (derived from 0 to 0 transitions) for a series of 17 TADF emitters. With respect to the experimental data, the optimally tuned RS functional leads to very good theoretical estimates with MADs of 0.15 eV for the $E_{VA}(S_1)$ values, 0.07 eV for the vertical ΔE_{ST} values, and 0.09 eV for the adiabatic ΔE_{ST}* values. In addition, high correlation coefficient values (R^2: 0.91, 0.85, and 0.93, respectively) are obtained. The plots of error distributions using the tuned functional present standard Gaussian shapes with the peak positions always around zero. The performance of the optimally tuned functional is clearly superior to that of the nontuned version, confirming the positive impact of the tuning. Commonly used RS functionals, such as ωB97XD and CAM-B3LYP, when considering default ω values, greatly overestimate the vertical excitation energies (MADs of > ∼0.5 eV) and produce relatively large MADs and relative errors for singlet−triplet gaps, which is mainly due to their high eX %. For non-RS functionals, both the pure GGA PBE functional and M06HF, which contain 0 and 100% eX, respectively, produce very large deviations (MADs > ∼1.0 eV for the vertical excitation energies and MADs > ∼0.20 eV for the singlet−triplet gaps), as well as large relative error values and low correlation coefficients. Compared to PBE and M06HF, hybrid functionals such as B3LYP and M062X overall give improved predictions, especially for the singlet−triplet gaps, which can be attributed to a suitable amount of eX; however, the good performance in predicting singlet−triplet gaps using M062X and B3LYP can be attributed to a simultaneous over/underestimation of the lowest singlet and triplet excitation energies.

To summarize, as it combines reliable estimates of the relevant energies with reasonable computational costs, an optimally tuned RS functional is seen as a useful tool in the design and prediction of novel TADF chromophores. In addition, because of its reliability in predicting both singlet and triplet excitation energies, an optimally tuned method can be explored for the description of singlet fission in organic semiconductors, which also requires quantitative assessments of singlet and triplet excited states.

■ ASSOCIATED CONTENT

Supporting Information

Introduction of the "Golden proportion" method, optimally tuned ω* values with different basis sets, calculated $E_{VA}(S_1)$ values using different PCM methods and basis sets, calculated $E_{VA}(S_1)$, ΔE_{ST}, and ΔE_{ST}* values using full TDDFT and TDA and using other density functionals, calculated relaxation energies, scheme regarding hole distributions of S_1 and T_1 for CBP and DPA-DPS, lowest singlet and triplet excitation assignments, histograms of calculated errors, linear correlation coefficients, and full names of the molecules investigated. The Supporting Information is available free of charge on the ACS Publications website at DOI: 10.1021/acs.jctc.5b00431.

■ AUTHOR INFORMATION

Corresponding Author

*E-mail: jean-luc.bredas@kaust.edu.sa.

Notes

The authors declare no competing financial interest.

■ ACKNOWLEDGMENTS

This work has been supported by King Abdullah University of Science and Technology (KAUST). We acknowledge the KAUST IT Research Computing Team for providing computational and storage resources and thank Dr. Bradley Rose and Dr. Yuan Li for stimulating discussions.

■ REFERENCES

(1) Bent, H. A. *Chem. Rev.* **1968**, *68*, 587−648.
(2) Brédas, J.-L. *Science* **1994**, *263*, 487−488.
(3) Tseng, H.-R.; Ying, L.; Hsu, B. B. Y.; Perez, L. A.; Takacs, C. J.; Bazan, G. C.; Heeger, A. J. *Nano Lett.* **2012**, *12*, 6353−6357.
(4) Yu, G.; Gao, J.; Hummelen, J. C.; Wudl, F.; Heeger, A. J. *Science* **1995**, *270*, 1789−1791.
(5) Lima, I. T.; Risko, C.; Aziz, S. G.; da Silva Filho, D. A.; Brédas, J.-L. *J. Mater. Chem. C* **2014**, *2*, 8873−8879.
(6) Uoyama, H.; Goushi, K.; Shizu, K.; Nomura, H.; Adachi, C. *Nature* **2012**, *492*, 234−238.
(7) Hirata, S.; Sakai, Y.; Masui, K.; Tanaka, H.; Lee, S. Y.; Nomura, H.; Nakamura, N.; Yasumatsu, M.; Nakanotani, H.; Zhang, Q.; Shizu, K.; Miyazaki, H.; Adachi, C. *Nat. Mater.* **2014**, *14*, 330−336.
(8) Nakanotani, H.; Higuchi, T.; Furukawa, T.; Masui, K.; Morimoto, K.; Numata, M.; Tanaka, H.; Sagara, Y.; Yasuda, T.; Adachi, C. *Nat. Commun.* **2014**, *5*, 4016.
(9) Tanaka, H.; Shizu, K.; Nakanotani, H.; Adachi, C. *Chem. Mater.* **2013**, *25*, 3766−3771.
(10) Huang, S.; Zhang, Q.; Shiota, Y.; Nakagawa, T.; Kuwabara, K.; Yoshizawa, K.; Adachi, C. *J. Chem. Theory Comput.* **2013**, *9*, 3872−3877.
(11) Friend, R. H.; Gymer, R. W.; Holmes, A. B.; Burroughes, J. H.; Marks, R. N.; Taliani, C.; Bradley, D. D. C.; Santos, D. A. D.; Brédas, J. L.; Logdlund, M.; Salaneck, W. R. *Nature* **1999**, *397*, 121−128.
(12) Zhang, Q.; Li, B.; Huang, S.; Nomura, H.; Tanaka, H.; Adachi, C. *Nat. Photonics* **2014**, *8*, 326−332.

(13) Chen, X.-K.; Zhang, S.-F.; Fan, J.-X.; Ren, A.-M. *J. Phys. Chem. C* **2015**, *119*, 9728−9733.
(14) Endo, A.; Ogasawara, M.; Takahashi, A.; Yokoyama, D.; Kato, Y.; Adachi, C. *Adv. Mater.* **2009**, *21*, 4802−4806.
(15) Dreuw, A.; Head-Gordon, M. *Chem. Rev.* **2005**, *105*, 4009−4037.
(16) Kánnár, D.; Szalay, P. G. *J. Chem. Theory Comput.* **2014**, *10*, 3757−3765.
(17) Samsonidze, G.; Jain, M.; Deslippe, J.; Cohen, M.; Louie, S. *Phys. Rev. Lett.* **2011**, *107*, 186404.
(18) Marques, M. A. L.; Ullrich, C. A.; Nogueira, F.; Rubio, A.; Burke, K.; Gross, E. K. U. *Time-Dependent Density Functional Theory*; Springer: Berlin, Germany, 2006; Vol. *706*.
(19) Runge, E.; Gross, E. K. U. *Phys. Rev. Lett.* **1984**, *52*, 997−1000.
(20) Autschbach, J. *ChemPhysChem* **2009**, *10*, 1757−1760.
(21) Dreuw, A.; Head-Gordon, M. *J. Am. Chem. Soc.* **2004**, *126*, 4007−4016.
(22) Autschbach, J.; Srebro, M. *Acc. Chem. Res.* **2014**, *47*, 2592−2602.
(23) Körzdörfer, T.; Brédas, J.-L. *Acc. Chem. Res.* **2014**, *47*, 3284−3291.
(24) Tozer, D. J. *J. Chem. Phys.* **2003**, *119*, 12697−12699.
(25) Yanai, T.; Tew, D. P.; Handy, N. C. *Chem. Phys. Lett.* **2004**, *393*, 51−57.
(26) Iikura, H.; Tsuneda, T.; Yanai, T.; Hirao, K. *J. Chem. Phys.* **2001**, *115*, 3540−3544.
(27) Sutton, C.; Sears, J. S.; Coropceanu, V.; Brédas, J.-L. *J. Phys. Chem. Lett.* **2013**, *4*, 919−924.
(28) Fonari, A.; Sutton, C.; Brédas, J.-L.; Coropceanu, V. *Phys. Rev. B: Condens. Matter Mater. Phys.* **2014**, *90*, 165205.
(29) Sun, H.; Autschbach, J. *ChemPhysChem* **2013**, *14*, 2450−2461.
(30) Savin, A., On degeneracy, near-degeneracy and density functional theory. In *Recent Developments and Applications of Modern Density Functional Theory*; Seminario, J. M., Ed.; Elsevier: Amsterdam, 1996; Vol. *4*, pp 327−357.
(31) Salzner, U.; Aydin, A. *J. Chem. Theory Comput.* **2011**, *7*, 2568−2583.
(32) Stein, T.; Kronik, L.; Baer, R. *J. Am. Chem. Soc.* **2009**, *131*, 2818−2820.
(33) Körzdörfer, T.; Sears, J. S.; Sutton, C.; Brédas, J.-L. *J. Chem. Phys.* **2011**, *135*, 204107−6.
(34) Sun, H.; Autschbach, J. *J. Chem. Theory Comput.* **2014**, *10*, 1035−1047.
(35) Stein, T.; Eisenberg, H.; Kronik, L.; Baer, R. *Phys. Rev. Lett.* **2010**, *105*, 266802.
(36) Baer, R.; Livshits, E.; Salzner, U. *Annu. Rev. Phys. Chem.* **2010**, *61*, 85−109.
(37) Levy, M.; Perdew, J. P.; Sahni, V. *Phys. Rev. A: At., Mol., Opt. Phys.* **1984**, *30*, 2745−2748.
(38) Kronik, L.; Stein, T.; Refaely-Abramson, S.; Baer, R. *J. Chem. Theory Comput.* **2012**, *8*, 1515−1531.
(39) Hirata, S.; Head-Gordon, M. *Chem. Phys. Lett.* **1999**, *314*, 291−299.
(40) Peach, M. J. G.; Williamson, M. J.; Tozer, D. J. *J. Chem. Theory Comput.* **2011**, *7*, 3578−3585.
(41) Peach, M. J. G.; Tozer, D. J. *J. Phys. Chem. A* **2012**, *116*, 9783−9789.
(42) Chantzis, A.; Laurent, A. D.; Adamo, C.; Jacquemin, D. *J. Chem. Theory Comput.* **2013**, *9*, 4517−4525.
(43) Moral, M.; Muccioli, L.; Son, W. J.; Olivier, Y.; Sancho-García, J. C. *J. Chem. Theory Comput.* **2015**, *11*, 168−177.
(44) Frisch, M. J.; Trucks, G. W.; Schlegel, H. B.; Scuseria, G. E.; Robb, M. A.; Cheeseman, J. R.; Scalmani, G.; Barone, V.; Mennucci, B.; Petersson, G. A.; Nakatsuji, H.; Caricato, M.; Li, X.; Hratchian, H. P.; Izmaylov, A. F.; Bloino, J.; Zheng, G.; Sonnenberg, J. L.; Hada, M.; Ehara, M.; Toyota, K.; Fukuda, R.; Hasegawa, J.; Ishida, M.; Nakajima, T.; Honda, Y.; Kitao, O.; Nakai, H.; Vreven, T.; Montgomery, J. A., Jr.; Peralta, J. E.; Ogliaro, F.; Bearpark, M. J.; Heyd, J.; Brothers, E. N.; Kudin, K. N.; Staroverov, V. N.; Kobayashi, R.; Normand, J.; Raghavachari, K.; Rendell, A. P.; Burant, J. C.; Iyengar, S. S.; Tomasi, J.; Cossi, M.; Rega, N.; Millam, N. J.; Klene, M.; Knox, J. E.; Cross, J. B.; Bakken, V.; Adamo, C.; Jaramillo, J.; Gomperts, R.; Stratmann, R. E.; Yazyev, O.; Austin, A. J.; Cammi, R.; Pomelli, C.; Ochterski, J. W.; Martin, R. L.; Morokuma, K.; Zakrzewski, V. G.; Voth, G. A.; Salvador, P.; Dannenberg, J. J.; Dapprich, S.; Daniels, A. D.; Farkas, Ö.; Foresman, J. B.; Ortiz, J. V.; Cioslowski, J.; Fox, D. J. *Gaussian 09*; Gaussian, Inc.: Wallingford, CT, USA, 2009.
(45) Tomasi, J.; Mennucci, B.; Cammi, R. *Chem. Rev.* **2005**, *105*, 2999−3094.
(46) Improta, R.; Barone, V.; Scalmani, G.; Frisch, M. J. *J. Chem. Phys.* **2006**, *125*, 054103.
(47) Tamblyn, I.; Refaely-Abramson, S.; Neaton, J. B.; Kronik, L. *J. Phys. Chem. Lett.* **2014**, *5*, 2734−2741.
(48) Perdew, J. P.; Schmidt, K. *AIP Conf. Proc.* **2001**, *577*, 1−20.
(49) Perdew, J. P.; Burke, K.; Ernzerhof, M. *Phys. Rev. Lett.* **1996**, *77*, 3865−3868.
(50) Becke, A. D. *J. Chem. Phys.* **1993**, *98*, 5648−5652.
(51) Lee, C.; Yang, W.; Parr, R. G. *Phys. Rev. B: Condens. Matter Mater. Phys.* **1988**, *37*, 785−789.
(52) Zhao, Y.; Truhlar, D. G. *Theor. Chem. Acc.* **2008**, *120*, 215−241.
(53) Zhao, Y.; Truhlar, D. G. *J. Phys. Chem. A* **2006**, *110*, 13126−13130.
(54) Vydrov, O. A.; Scuseria, G. E. *J. Chem. Phys.* **2006**, *125*, 234109.
(55) Chai, J.-D.; Head-Gordon, M. *J. Chem. Phys.* **2008**, *128*, 084106.
(56) Jacquemin, D.; Perpète, E. A.; Ciofini, I.; Adamo, C. *J. Chem. Theory Comput.* **2010**, *6*, 1532−1537.
(57) Beljonne, D.; Shuai, Z.; Friend, R. H.; Brédas, J. L. *J. Chem. Phys.* **1995**, *102*, 2042−2049.
(58) Beljonne, D.; Cornil, J.; Friend, R. H.; Janssen, R. A. J.; Brédas, J. L. *J. Am. Chem. Soc.* **1996**, *118*, 6453−6461.
(59) Cohen, A. J.; Mori-Sánchez, P.; Yang, W. *Science* **2008**, *321*, 792−794.
(60) Körzdörfer, T.; Parrish, R. M.; Marom, N.; Sears, J. S.; Sherrill, C. D.; Brédas, J.-L. *Phys. Rev. B: Condens. Matter Mater. Phys.* **2012**, *86*, 205110.
(61) Valiev, M.; Bylaska, E. J.; Govind, N.; Kowalski, K.; Straatsma, T. P.; Van Dam, H. J. J.; Wang, D.; Nieplocha, J.; Apra, E.; Windus, T. L.; de Jong, W. A. *Comput. Phys. Commun.* **2010**, *181*, 1477−1489.

DOI: 10.1021/acs.jctc.5b00431
J. Chem. Theory Comput. 2015, 11, 3851−3858